Early age behaviour of concrete nuclear containments

Farid Benboudjema, Jean-Michel Torrenti

EARLY AGE BEHAVIOUR OF CONCRETE NUCLEAR CONTAINMENTS

F. Benboudjema [(1)], J.M. Torrenti [(1 & 2)]

(1) ENS Cachan/CNRS UMR8535/UPMC/PRES UniverSud Paris, Cachan, France

(2) Laboratoire Central des Ponts et Chaussées, Paris, France

Keywords: early-age; cracking; creep; temperature; hydration; shrinkage.

Abstract

A numerical model has been developed to predict early age cracking for massive concrete structures. Taking into account creep at early-age is essential if one wants to predict quantitatively the induced stresses if autogenous or thermal strains are restrained. Because creep strains may relax internal stresses, a creep model which includes the effects of hydration and temperature is used. For the prediction of cracking, a simple elastic damage model is used. Numerical simulations are performed in order to predict the behaviour of a massive wall and a concrete containment of a nuclear power plant. They show that significant relaxation of stresses (due to creep) occurs only after about ten days, after cracking occurs. Moreover, since temperature in concrete may reach important values in massive concrete structures, it appears that effect of temperature on creep must be taken into account for an accurate prediction of cracking.

1. INTRODUCTION

Concrete containments of nuclear power plants are very massive structures. During the construction, concrete lifts are about 3 m high, and the duration between lifts is about 15 days. Two important phenomena are likely to occur:

- Because the thickness of concrete is equal to 1.2 m, and due to the release of heat during the hydration reaction, a temperature gradient is generated inside the wall, which will induce differential evolutions of hydration degree, thermal strains and autogenous strains. While the material does not exhibit a sufficient stiffness, induced stresses are very small (compared to the strength). However, as soon as the stiffness becomes to increase, stresses appear and cracking may develop;
- The concrete layer, which is going to be cast, exhibit thermal and autogenous strains, while the strains of the concrete layer, previously cast, are, at this time, no more significant. Furthermore, the Young modulus of each concrete layer is different. Therefore, the strains in the youngest concrete layer are restrained (by the oldest concrete layer) and tensile stresses arise.

Besides these 2 effects, differential strains occur between concrete and reinforcement, which can lead to micro-cracking. This has not been taken into account in this study.

Early-age cracks may close partially or totally, due to relaxation and further applied prestress. However, they may reopen later, in the case of an accident, and thus promote the leakage of radioactive elements in the environment, during the service life of the containments. Therefore, it is important to predict initial stresses in the structure, before the application of the prestress, in order to evaluate the potential risks.

The prediction of cracking needs a numerical resolution due to the complexity of the behaviour of concrete at early-age. The following phenomena must be taken into account:

- The evolution of hydration: this is achieved here by the use of a chemical affinity (Ulm and Coussy, 1998);
- The evolution of temperature: the energy balance equation, which includes the release of heat due to the hydration reaction is solved;
- The evolutions of autogenous and thermal strains;
- The evolution of Young modulus and tensile strength with respect to the hydration degree;
- The description of cracking in tension: an existing elastic damage model is slightly modified (Mazars, 1986);
- Basic and thermal transient creep strains, affected by hydration degree and temperature;
- Drying shrinkage and drying creep: theses features can be neglected since we focus only on massive structures at early-age. Indeed, drying process is 1000 to 10000 times slower than the thermal one. Minor micro-cracking due to differential drying shrinkage is expected to occur during the first days.

Several models have been proposed in order to study the early-age behaviour of massive concrete structures by means of finite element calculations. Xiang et *al.* (2005) performed a thermo-elastic analysis using time dependant evolutions of release of heat (due to hydration) and material properties. Ayotte et *al.* (1997) used a commercial finite element code to perform also a thermo-elastic analysis, and again all properties are made dependant explicitly on time

(and not hydration degree or equivalent time), which is not totally accurate when temperature is not constant. De Borst and van den Boogaard (1995), Niu et *al.* (1995), Meschke (1996) used also rather empirical material models, but they had incorporated in their model basic creep and cracking. Aggoun et *al.* (1994), Waller et *al.* (2004) used the maturity concept and perform thermo-elastic analyses using the commercial finite element code CESAR-LCPC. Mazars and Bournazel (1996) used also the maturity concept; nevertheless they used an elastic damage model for cracking. A similar approach, with the take into account of creep strains, has been achieved by Hattel and Thorborg (2003). Ulm and Coussy (1998), Lackner and Mang (2004) used a chemoplastic model, without taking into account creep strain. Faria et *al.* (2006) used a similar approach for the chemo-thermal equations, but they take also into account basic creep, but not cracking. Cervera et *al.* (1999) used also theory of reactive porous media, with the prediction of damage and creep. De Schutter (2002a, 2002b) takes into account creep, but a simple stress based cracking criterion was used and temperature effect on creep has not been taken into account. From these observations, it seems that none of the aforementioned models incorporated, at the same time, hydration, thermal, autogenous shrinkage, (basic and thermal transient) creep and cracking. Besides, in some models, materials properties (Young modulus, strengths, fracture energy, creep) are taken explicitly dependant on time, which is not correct. Indeed, these properties depend rather on hydration degree (or maturity or equivalent time). For thin structures (where temperature evolution is not such important), using time or hydration degree may lead to similar results. However, for massive structures (which is our concern, here), different results may be predicted.

Therefore, in this paper, a model, which takes into account aforementioned phenomena, is presented. Materials properties are taken, explicitly, dependant of hydration degree which is

consistent with experimental evidences (e.g. Byfors, 1980; Laplante and Boulay, 1994; Springenschmidt, 1998; De Schutter, 1999). It has been implemented in a finite elements code (Cast3m, developed by the French Atomic Energy Commission). Numerical simulations are performed and compared to experimental ones obtained by EDF (French Group of electricity) (Mazars and Bournazel, 1996; Ithurralde, 1989) on two massive wall (cast with an ordinary and high performance concrete). The objective is to show the ability of the model to predict chemo-thermo-mechanical behaviour of concrete at early-age. A parametric study is also performed to show the effect of creep coupled with hydration and temperature on the numerical simulations.

2. CONSTITUTIVE MODEL

2.1 Chemo-thermal model

The hydration of cement paste is a thermo-activated process, which can be taken into account through an Arrhenius type law (e.g. Regourd and Gauthier, 1980). Its evolution is modelled by the following relation (Ulm and Coussy, 1998; Lackner and Mang, 2004):

$$\dot{\xi} = \tilde{A}(\xi)\exp\left(-\frac{E_a}{RT}\right) \tag{1}$$

in which $\dot{\xi}$ is the rate of degree of hydration , $\tilde{A}(\xi)$ is the normalized affinity, E_a is the activation energy [J.mol^{-1}], R is the constant of perfect gas [8.314 J.mol^{-1}.K^{-1}] and T is the temperature in Kelvin. The normalized affinity is associated to the micro-diffusion process of water which reacts with unhydrated cement (Ulm and Coussy, 1998). The activation energy is found to be dependent on temperature and measurement methods (e.g., D'aloia and Chanvillard, 2002; Schindler, 2004). This is due to the fact that several chemical reactions, with different kinetics, occur during hydration of cement. However, it is assumed here, in the

same way that most of models, that this parameter is constant, since its evolution of temperature depends also on the type of cement (for which no information are available).

The evolution of temperature is obtained from the energy balance equation, which includes the release of heat due to the hydration reaction:

$$C\dot{T} = \nabla\left(k\nabla T\right) + L\dot{\xi} \tag{2}$$

in which L is the latent heat of hydration [J.m^{-3}], k is the thermal conductivity [W.m^{-1}.K^{-1}] and C in volumetric heat capacity [J.m^{-3}.K^{-1}], which could be kept constant (Waller, 2000). The parameter L and the normalized affinity $\tilde{A}(\xi)$ can be obtained experimentally by measuring the temperature during an adiabatic or a quasi-adiabatic test.

The boundary conditions are assumed to be of convective type. The convective heat flux $\boldsymbol{\varphi}$ [W.m^{-2}] reads:

$$\varphi = h\left(T_s - T_{ext}\right)\mathbf{n} \tag{3}$$

where h is the coefficient of exchange by convection [W.m^{-2}.K^{-1}], T_s is the temperature on the surface [K]; T_{ext} is the ambient temperature [K] and $\mathbf{n}$ is the normal unit vector to the surface (oriented towards the exterior).

2.2 Autogenous and thermal shrinkage model

Due to Le Chatelier contraction (the volume of the reactants is higher than the volume of the new products), porosity filled with air and water arises during hydration of concrete. This leads to the self-desiccation of the material and therefore to the rise of capillary pressures in the material. As concrete hardens, autogenous shrinkage develops. Autogenous shrinkage is therefore related to the evolution of hydration in the material. Experimental results show that autogenous shrinkage evolution is linear with respect to the hydration degree as soon as a

threshold has been overcame (e.g. Laplante, 1993; Mounanga et *al.*, 2006). Therefore, autogenous shrinkage $\boldsymbol{\varepsilon}_{au}$ can be modelled by (e.g. Ulm and Coussy, 1998):

$$\dot{\boldsymbol{\varepsilon}}_{au} = -\kappa\dot{\xi}\mathbf{1} \text{ for } \xi > \xi_0 \tag{4}$$

where κ is a constant material parameter, $\mathbf{1}$ is the unit tensor and ξ_0 is a threshold (see Eq. 7).

An expansion can also be measured at the beginning of hydration, depending of the w/c ratio and type of cement. This is not taken into account here. Besides, more accurate approaches are available, where autogenous shrinkage is related directly to the elastic and creep deformation of the skeleton submitted to capillary pressure (build by self-dessiccation) (e.g. Michaud, 2007; Pichler et *al.*, 2007). However, they require an extensive experimental program to identify material parameters.

The thermal strain $\boldsymbol{\varepsilon}_{th}$ is related to the temperature variation, due to the release of heat by the hydration, and to the coefficient of thermal expansion α, which is considered to be constant:

$$\dot{\boldsymbol{\varepsilon}}_{th} = \alpha\dot{T}\mathbf{1} \tag{5}$$

Experimental results show that this is, in reality, very difficult to separate autogenous and thermal strains at early age. For instance, both autogenous shrinkage and coefficient of thermal expansion depend upon temperature (e.g. Laplante 1993; Bjøntegaard 1999; Turcry and Loukili, 2002; Mounanga et *al.*, 2006) and relative humidity (e.g. Bjøntegaard 1999), as the coefficient of thermal expansion may also depends upon hydration degree (due to the formation of new products and phase change). Relative humidity at early age affects only a few centimetres of thick concrete structure. Laplante (1993) founds that the coefficient of thermal expansion of concrete evolves dramatically during the first 14 hours (in term of

maturity) and then stabilizes. This result has been confirmed by several authors (e.g. Loukili et *al.*, 2000; Sarkis et *al.*, 2002). In this work, we focus only on the behaviour of concrete after setting. Besides, these couplings are not well understood, yet. Therefore, these features are not taken into account.

2.3 Elastic-damage model

The mechanical behaviour of concrete is modelled by an elastic-damage model coupled with creep, which includes the evolution of the elastic stiffness with respect to the hydration degree (taking from de Schutter, 1999) and with respect to damage (Mazars, 1986). This model allows for predicting correctly degradation of the material in tension; however it is not suitable for describing dilatancy and behaviour for high biaxial/triaxial compressive stresses. Since cracking occurs mainly in tension at early-age (due to the restrain of strains), the adopted model seems to be the best compromise (between complexity and accuracy).

The relationship between apparent stresses $\boldsymbol{\sigma}$, effective stresses $\tilde{\boldsymbol{\sigma}}$, damage D, elastic stiffness tensor $\mathbf{E}$, elastic strains $\boldsymbol{\varepsilon}_e$, basic creep strains $\boldsymbol{\varepsilon}_{bc}$, transient thermal creep strains $\boldsymbol{\varepsilon}_{ttc}$, total strains $\boldsymbol{\varepsilon}$, and previously defined strains reads:

$$\boldsymbol{\sigma} = (1-D)\tilde{\boldsymbol{\sigma}} \text{ and } \dot{\tilde{\boldsymbol{\sigma}}} = \mathbf{E}(\xi)\dot{\boldsymbol{\varepsilon}}_{el} = \mathbf{E}(\xi)\left(\dot{\boldsymbol{\varepsilon}} - \dot{\boldsymbol{\varepsilon}}_{bc} - \dot{\boldsymbol{\varepsilon}}_{ttc} - \dot{\boldsymbol{\varepsilon}}_{au} - \dot{\boldsymbol{\varepsilon}}_{th}\right) \tag{6}$$

The Poisson ratio is assumed to be constant and the Young modulus E increases due to hydration as follows (De Schutter, 1999):

$$E(\xi) = E_\infty \bar{\xi}^{\beta} \text{ with } \bar{\xi} = \left\langle \frac{\xi - \xi_0}{\xi_\infty - \xi_0} \right\rangle_+ \tag{7}$$

in which ξ_0 the mechanical percolation threshold: it corresponds to the hydration degree below the concrete has negligible mechanical properties (Young modulus, strength …). It is

closely related to the setting time. It is kept constant and equal to 0.1, which corresponds to the usual value reported in the bibliography analysis of de Schutter and Taerwe (1996). However, it depends, in fact, on the aggregate content, type of cement and water to cement ratio (Torrenti and Benboudjema, 2005). ξ_∞ is the final hydration degree, E_∞ is the final Young modulus (i.e. when $\xi = \xi_\infty$) and β is a constant equal to 0.62 according to De Schutter (1999). $\langle\cdot\rangle_+$ is the positive part operator.

D is linked to the elastic equivalent tensile strain $\hat{\varepsilon}$:

$$\hat{\varepsilon} = \sqrt{\langle \boldsymbol{\varepsilon}_{el} \rangle_+ : \langle \boldsymbol{\varepsilon}_{el} \rangle_+} \tag{8}$$

The damage criterion is given by (Mazars, 1986):

$$f = \hat{\varepsilon} - \kappa_0(\xi) \tag{9}$$

Where $\kappa_0(\xi)$ is the tensile strain threshold. Then, $\dot{D} = 0$ if $\hat{\varepsilon} \leq \kappa_0(\xi)$ and:

$$D = 1 - \frac{\kappa_0}{\hat{\varepsilon}}\left[(1 + A_t)\exp(-B_t\hat{\varepsilon}) - A_t \exp(-2B_t\hat{\varepsilon})\right] \text{ if } \hat{\varepsilon} \geq \kappa_0\ (\xi) \tag{10}$$

where A_t and B_t are constant material parameters which controls the softening branch in the stress-strain curve in tension.

In our application we consider only damage due to tension (compressive stresses are very small in compared with the compressive strength). The tensile strength evolution reads (De Schutter, 1999):

$$f_t(\xi) = f_{t\infty}\bar{\xi}^{\gamma} \tag{11}$$

where $f_{t\infty}$ [Pa] is the final tensile strength (i.e. when $\xi = \xi_\infty$). For a CEM I 52.5, De Schutter and Taerwe (1997) found that $\gamma = 0.46$ fits well experimental data.

The evolution of the tensile strain threshold is then computed from the evolution of tensile strength (Eq. 11) and the Young modulus (Eq. 7):

$$\kappa_0(\xi) = \frac{f_t(\xi)}{E(\xi)} = \frac{f_{t\infty}}{E_\infty}\,\bar{\xi}^{\gamma-\beta} \tag{12}$$

Strain softening induces inherent mesh dependency and produces failure without energy dissipation (Pijaudier-Cabot et *al.*, 1987). In order to avoid such shortcomings, a characteristic length l_c is introduced. This length is related to the mesh size (Rots 1988, Cervera and Chiumenti 2006) in order to dissipate the same amount of energy after mesh refinement, when strains localize in one row of finite elements.

For the adopted model, the dissipated energy density g_{ft} at failure in tension reads:

$$g_{ft}(\xi) = \frac{f_t(\xi)(1 + A_t/2)}{B_t} \tag{13}$$

It is related to the fracture energy G_{ft} and the characteristic length l_c:

$$g_{ft}(\xi) = \frac{G_{ft}(\xi)}{l_c} \tag{14}$$

The fracture energy depends on the hydration degree (De Schutter et Taerwe, 1997):

$$G_{ft}(\xi) = G_{ft\infty}\,\bar{\xi}^{\delta} \tag{15}$$

For a CEM I 52.5, De Schutter et Taerwe (1997) found that $\delta = 0.46$ fits well experimental data.

2.3 Basic creep model

Models for basic creep are, usually, based on rheological elements (spring and dashpots): Kelvin-Voigt and Maxwell chains are combined in serial or/and parallel. Hauggaard et *al.*

(1999) and de Schutter (1999) used only one Kelvin-Voigt unit for the modelling of early-age basic creep. Several authors (e.g. Lokhorst and Breugel, 1997; Mabrouke et *al*. 2004) improved the model of Bazant and Prasannan (1989) based on solidification theory. Bazant et *al.* (1997) improved also this model by considering that the effect of age (even when hydration reaction does not evolve anymore) is due also to the relaxation of micro-prestress. By assuming that the micro-prestress relaxation depends also on relative humidity and temperature, this model can also predict drying and transient thermal creep. The development of the micro-prestress is found also dependant, in a great extent, on the type of concrete.

Here, we used several Kelvin-Voigt chains (see Figure 1). We will show that the use of such elements gives straightforward formula for the computations of strain evolution, in contrary to Maxwell chains for instance, which need the use of an algorithm (such as the so called exponential algorithm proposed by Bazant and Wu, 1974). The incremental constitutive relation for an aging spring was shown in Bazant (1998) to be the only possible one which does not violate thermodynamic restrictions. It will be adopted here.

Let us consider a Kelvin-Voigt unit *i*. The incremental equilibrium equation for the Kelvin cell is:

$$\dot{\tilde{\sigma}} = \dot{\tilde{\sigma}}^i_{sp} + \dot{\tilde{\sigma}}^i_{ds} \tag{16}$$

where $\tilde{\sigma}^i_{ds}$ and $\tilde{\sigma}^i_{sp}$ are the effective stresses acting on the dashpot and the spring (in the Kelvin-Voigt unit *i*), respectively.

The behaviour law of the spring reads:

$$k^i_{bc}(\xi)\dot{\varepsilon}^i_{bc} = \dot{\tilde{\sigma}}^i_{sp} \tag{17}$$

where ε_{bc}^{i} is the elementary basic creep strain and k_{bc}^{i} is the stiffness of the spring in the Kelvin-Voigt unit *i*.

The behaviour law of the dashpot reads:

$$\eta_{bc}^{i}(\xi)\dot{\varepsilon}_{bc}^{i} = \tilde{\sigma}_{ds}^{i} \tag{18}$$

where η_{bc}^{i} is the viscosity of the dashpot in the Kelvin-Voigt unit *i*.

Hauggaard et *al.* (1999) expresses material parameters as functions of time. The effect of age on basic creep of concrete is, here, taken into account by relating the material parameters to the degree of hydration, since it is more physical (see introduction). The relationships proposed by de Schutter (1999) are slightly modified for the Kelvin-Voigt units:

$$\begin{cases} k_{bc}^{i}(\xi) = k_{bc\_\infty}^{i} \dfrac{0.473}{2.081 - 1.608\bar{\xi}} \bar{\xi}^{0.62} \\ \tau_{bc}^{i} = \dfrac{\eta_{bc}^{i}(\xi)}{k_{bc}^{i}(\xi)} \end{cases} \tag{19}$$

where $k_{bc\_\infty}^{i}$ is the final stiffness (i.e. when $\xi = \xi_{\infty}$) of the spring in the Kelvin-Voigt unit *i*.

The retardation times τ_{bc}^{i} are assumed to be constant.

Combining Eq. (16), Eq. (17) and Eq. (18), we obtain a non-linear second order differential equation for each Kelvin-Voigt element:

$$\tau_{bc}^{i}\ddot{\varepsilon}_{bc}^{i} + \left(\tau_{bc}^{i}\frac{\dot{k}_{bc}^{i}(\xi)}{k_{bc}^{i}(\xi)} + 1\right)\dot{\varepsilon}_{bc}^{i} = \frac{\dot{\tilde{\sigma}}}{k_{bc}^{i}(\xi)} \tag{20}$$

The effect of temperature on creep must be taken into account. Experimental results highlight that temperature increases creep at early-age by a factor of 2-3 (Arthanari and Yu, 1967). It is twofold. In one hand, temperature evolution increases rate of hydration degree, and therefore

reduces creep strains at higher temperature. Indeed, if the temperature increases, the hydration (Eq. 1) and therefore the spring stiffness increase also (Eq. 19). The result is a decrease of creep strain rate with respect to temperature. This is in contradiction with experimental evidences. In the other hand, temperature increases creep strains due to the two following factors (Hauggaard et *al.*, 1999):

- At constant temperature, creep strains rate increases. This is due to the decrease of water viscosity with temperature;
- Transient temperature history increases also creep strains. The obtained deformation is called transient thermal creep or load induced thermal strains. Such kind of strain is also observed at very high temperature (above 100°C). Bazant et *al.* (1997) suggest that this strain correspond to drying creep.

In order to separate these mechanisms, creep strains have to be measured at different constant temperatures and for different temperature history.

The effect of constant temperature on creep strain is taken into account by modifying the spring stiffness and the dashpot viscosity of Kelvin-Voigt units as follows:

$$k_{bc}^{i}(\xi,T)=k_{bc}^{i}(\xi,T_0)e^{\frac{E_{ac}}{R}\left(\frac{1}{T}-\frac{1}{T_0}\right)} \text{ and } \eta_{bc}^{i}(\xi,T)=\eta_{bc}^{i}(\xi,T_0)e^{\frac{E_{ac}}{R}\left(\frac{1}{T}-\frac{1}{T_0}\right)} \quad (21)$$

Where E_{ac} is the creep activation energy and T_0 = 293 K. In this way, the characteristic time is kept independent of the temperature.

The creep activation energy has been fitted on experimental results of Arthanari and Yu (1967), plotted in Figure 2. The specimens were loaded at an age of 15 days at 6.9 MPa in compression, and heats one day before at a constant temperature (20, 40 and 62 °C). A value of E_{ac} = 17.4 kJ.mol^{-1} has been obtained, and it will be kept for all the following calculations.

This value is very close to the activation energy for the water viscosity (16.4 kJ.mol^{-1}) and to the one used by Hauggard et *al.* (1999, 16 kJ.mol^{-1}). However, there is a difference with Hauggard et *al.* (1999) calculations, since they did not consider an evolution of spring stiffness with respect to temperature. If one considers only an evolution of the viscosity, one could not fit correctly anymore experimental results of Arthanari and Yu (1967).

Hauggard et *al.* (1999) have modeled transient thermal creep by using the model developed by Bazant et *al.* (1997). Here, a more simple model is used which is similar to the one used to predict thermal transient creep of concrete at high temperatures (Thelandersson, 1987). Thermal transient creep strain ε_{ttc} reads:

$$\dot{\varepsilon}_{ttc} = \lambda \left| \dot{T} \right| \tilde{\sigma} \tag{22}$$

where λ [Pa^{-1}.K^{-1}] is a material parameter. This expression can be also obtained from the microprestress model by considering that the microprestress rate is equal to the temperature rate.

A value of λ = 1.38×10^{-12} Pa^{-1}.K^{-1} fits well experimental data of Hauggard et *al.* (1999, see Fig. 3). This value is also close to the one fitted from thermal transient creep experiments at high temperatures (Thelandersson, 1987). It should be noted that Eq. (22) implies that transient thermal creep occurs in the same manner during heating and cooling, which seems to be consistent with experimental data of Hauggard et *al.* (1999). However, if several heating/cooling cycles are considered, Eq. (22) predicts a continuous increase of strains, which may not be consistent. Therefore, this model should not be used in that case.

The creep models are then extended to multiaxial state of stresses by mean of a creep Poisson ratio taken equal to the elastic one. Besides, predicted creep strains are assumed to be the

same in compression and tension, altougth this question is not fully resolved yet. This assumption is consistent with some experimental results (Ostergaard et *al.*, 2001; Gutsch, 2002) which show that compressive and tensile creep strains evolves almost identically at early-age. However, recent extensive research work of Atrushi (2003) concluded that creep in tension is lower than in compression initially, but the creep rate is soon much higher in tension than in compression.

2.4 Numerical algorithm

The non linear constitutive equations need the use of an algorithm. In order to compute creep strains, the effective stresses are linearized, for each time step:

$$\tilde{\boldsymbol{\sigma}}(t) = \tilde{\boldsymbol{\sigma}}_n + \Delta\tilde{\boldsymbol{\sigma}}_{n+1}\frac{(t-t_n)}{\Delta t_n} \tag{23}$$

with $t \in [t_n; t_{n+1}]$, $\Delta t_n = t_{n+1} - t_n$, $\Delta\tilde{\boldsymbol{\sigma}}_{n+1} = \tilde{\boldsymbol{\sigma}}_{n+1} - \tilde{\boldsymbol{\sigma}}_n$ and where t_n is the time at time-step number n; $\tilde{\boldsymbol{\sigma}}_n$ is the effective stress at time step number n.

Since Eq. (20) is non linear, the spring stiffness is assumed to be constant within each time step and equal to their mean values:

$$k_{bc}^i(\xi,T) \approx \hat{k}_{bc}^i = k_{bc}^i\left(\frac{\xi_n+\xi_{n+1}}{2}, \frac{T_n+T_{n+1}}{2}\right) \;\&\; \dot{k}_{bc}^i(\xi,T) \approx \hat{\dot{k}}_{bc}^i = \frac{k_{bc}^i(\xi_{n+1},T_{n+1}) - k_{bc}^i(\xi_n,T_n)}{\Delta t_n}$$

$$\text{for } \xi \in [\xi_n;\xi_{n+1}] \;\&\; T \in [T_n;T_{n+1}] \tag{24}$$

Then, basic creep strains are expressed as (after solving the differential equation (20)):

$$\Delta\varepsilon_{bc}^{n+1} = \varepsilon_{bc}^{n+1} - \varepsilon_{bc}^{n} = a_{bc} + b_{bc}\cdot\tilde{\sigma}_n + c_{bc}\cdot\tilde{\sigma}_{n+1} \tag{25}$$

where $\boldsymbol{\varepsilon}_{bc}^n$ is the basic creep strains vector at time-step number n; a_{bc}, b_{bc} and c_{bc} are depend only upon material parameters and Δt_n:

$$\begin{cases} a_{bc} = -\sum_i \dfrac{\tilde{\sigma}^i_{dsn}}{\underline{k}^i_{bc}} \left(e^{-\frac{\Delta t_n}{\underline{\tau}^i_{bc}}} - 1 \right) \\ b_{bc} = -\sum_i \dfrac{1}{\underline{k}^i_{bc}} \left[1 + \dfrac{\underline{\tau}^i_{bc}}{\Delta t_n} \left(e^{-\frac{\Delta t_n}{\underline{\tau}^i_{bc}}} - 1 \right) \right] \text{ with } \begin{cases} \underline{k}^i_{bc} = \omega_i \hat{k}^i_{bc} \\ \underline{\tau}^i_{bc} = \dfrac{\tau^i_{bc}}{\omega_i} \\ \omega_i = 1 + \hat{k}^i_{bc} \dfrac{\tau^i_{bc}}{\hat{k}^i_{bc}} \end{cases} \\ c_{bc} = -b_{bc} \end{cases} \tag{26}$$

The stress in the dashpot is then updating at the end of each time step:

$$\tilde{\sigma}^i_{dsn+1} = \Delta\tilde{\sigma}_{n+1} \frac{\underline{\tau}^i_{bc}}{\Delta t_n} \left(1 - e^{-\frac{\Delta t_n}{\underline{\tau}^i_{bc}}} \right) + \tilde{\sigma}^i_{dsn} e^{-\frac{\Delta t_n}{\underline{\tau}^i_{bc}}} \tag{27}$$

Therefore, we only need to know the stresses and the creep strains at time step number n to calculate the creep strains at time-step number $n+1$ (the storage of the stress history is not needed).

Eq. (25) is extended in 3D, by mean of a creep Poisson ratio (which has been taken equal to the elastic one):

$$\Delta\boldsymbol{\varepsilon}^{n+1}_{bc} = \mathbf{A}_{bc} + \mathbf{B}_{bc} \cdot \tilde{\boldsymbol{\sigma}}_n + \mathbf{C}_{bc} \cdot \tilde{\boldsymbol{\sigma}}_{n+1} \tag{28}$$

Thermal transient creep increment reads:

$$\Delta\varepsilon^{n+1}_{ttc} = \varepsilon^{n+1}_{ttc} - \varepsilon^{n}_{ttc} = t_{ttc} \cdot \left(\tilde{\sigma}_n + \tilde{\sigma}_{n+1} \right) \text{ with } t_{ttc} = \lambda \frac{\left(T_{n+1} - T_n \right)}{2} \tag{29}$$

Eq. (29) is also extended in 3D, in the same way than basic creep:

$$\Delta\boldsymbol{\varepsilon}^{n+1}_{ttc} = \mathbf{T}_{ttc} \cdot \left(\tilde{\boldsymbol{\sigma}}_n + \tilde{\boldsymbol{\sigma}}_{n+1} \right) \tag{30}$$

The effective stresses increment $\Delta\tilde{\boldsymbol{\sigma}}_{n+1}$ at the end of the time step number n is updated by the following relationship:

$$\Delta\tilde{\boldsymbol{\sigma}}_{n+1} = \mathbf{E}\cdot\Delta\boldsymbol{\varepsilon}_e^{n+1} = \mathbf{E}\cdot\left(\Delta\boldsymbol{\varepsilon}^{n+1} - \Delta\boldsymbol{\varepsilon}_{bc}^{n+1} - \Delta\boldsymbol{\varepsilon}_{au}^{n+1} - \Delta\boldsymbol{\varepsilon}_{th}^{n+1} - \Delta\boldsymbol{\varepsilon}_{ttc}^{n+1}\right) \tag{31}$$

Finally, if one makes use of Eqs. (28) and (30), the effective stresses vector increment $\Delta\tilde{\boldsymbol{\sigma}}_{n+1}$ reads:

$$\Delta\tilde{\boldsymbol{\sigma}}_{n+1} = \mathbf{E}_c\cdot\left(\Delta\boldsymbol{\varepsilon}^{n+1} - a_{bc}\boldsymbol{\varepsilon}_{bc}^{n} - \left(\mathbf{B}_{bc} + \mathbf{C}_{bc} + \mathbf{T}_{ttc}\right)\cdot\tilde{\boldsymbol{\sigma}}_n - \Delta\boldsymbol{\varepsilon}_{au}^{n+1} - \Delta\boldsymbol{\varepsilon}_{th}^{n+1}\right) \tag{32}$$

With:

$$\mathbf{E}_c = \left(\mathbf{1} + \mathbf{E}\cdot\left(\mathbf{C}_{bc} + \mathbf{T}_{ttc}\right)\right)^{-1}\cdot\mathbf{E} \tag{33}$$

Then, the elastic strain is computed:

$$\boldsymbol{\varepsilon}_e^{n+1} = \boldsymbol{\varepsilon}_e^{n} + \Delta\boldsymbol{\varepsilon}_e^{n+1} \text{ with } \Delta\boldsymbol{\varepsilon}_e^{n+1} = \mathbf{E}^{-1}\Delta\tilde{\boldsymbol{\sigma}}_{n+1} \tag{34}$$

The equivalent tensile strain and the damage variable are calculated using Eq. (8) and (10). Finally, the apparent stresses are calculated by Eq. (6). The algorithm is summarized in Figure 4.

Therefore, the numerical implantation is straightforward. Indeed, all involved equations are defined analytically and can be calculated without any local iteration, which enhances the speed of calculations. Moreover, there is no need to store the whole history of stresses and strains for the computation of creep strain. Only, temperature, hydration degree, previous creep strains and stresses are needed.

3. NUMERICAL SIMULATION OF A CONTAINMENT

3.1 Introduction

During the construction of the Civaux nuclear power plant, two reinforced concrete wall (with prestressing cable ducts) were built in order to evaluate the risk of cracking of the real containment at early age, using two different concrete mixes: an ordinary concrete (OC) and a

high performance concrete (HPC). The walls were both 1.2 m wide, 1.9 m high, 20 m long and were equipped with thermocouples in order to follow the evolution of the temperatures in different locations (see Figure 5). Table 1 gives the two concretes mixes (Ithurralde, 1989).

3.2 Thermal simulations of the wall

Because of the length of the wall, we can assume that the problem is a planar one. Only half of the wall has been meshed for the finite elements calculations due to the symmetry of the structure (see Figure 5). A constant exchange coefficient h at the surface of concrete is assumed. On the symmetry axis, the heat flux is equal to zero. The initial temperature in the wall is taken equal to 20°C, as it is taken equal to 7°C in the slab. The external temperature is kept constant and equal to 10°C. Since the slab has been previously cast, it is assumed that only thermal diffusion occurs (there is no more hydration and associated release of heat). Therefore, only the wall hydrates and releases heat (due to hydration).

It is recall that in order to calibrate correctly the chemical affinity (Eq. 1) and the latent heat of hydration (Eq. 2), evolution of temperature in an adiabatic or quasi-adiabatic test must be recorded. However, such experimental data were not available for the studied concretes. Therefore, experimental semi-adiabatic results obtained on similar concrete mixes are used. They have been slightly modified in order to retrieve a correct evolution of recorded temperature in the wall. The identified affinity (with respect to hydration degree) for both concrete mixes is plotted in Figure 6.

Figures 7 and 8 show the evolutions of experimental and simulated temperatures at different locations (see Fig. 5 for the location of the dots). Temperature field, after 25 hours, is reported in Figure 9. The thermal parameters are given in Table 2. It should be emphasized

that the thermal conductivity is very important here since the wall is highly reinforced (which is the case for containments of nuclear power plants).

The numerical simulations give reasonable results in term of maximum temperature reached in the core and the surface, for both concretes. A maximal temperature of 59 °C after 25 hours and 46 °C after 36 hours is reached for the OC and the HPC concrete, respectively. However, the decreasing of temperature is not accurately predicted for the OC.

Moreover, the maximum temperature is reached in the OC wall (and not in the HPC wall). This is not usual. This is due to the fact, that the HPC have been specially designed (Larrard et *al.*, 1992) in order to limit the release of hydration heat. Indeed, its mix (Table 1) shows a low content of cement and the use of limestone filler.

3.3 Basic creep calculations

Experimental creep data for both concretes are not available at early-age. Therefore, experimental results of Laplante (1993), obtained on concrete with similar mixes, are used. Tests were performed on Φ 300 × 1200-mm cylindrical columns. After the form removal, the specimens were covered with self-adhesive aluminium sheets to prevent drying. Thus, only elastic strain, creep strain, autogenous and thermal shrinkage are concerned. The specimens were loaded at an age of 20 hours and submitted to a stress history reported in Fig. 10 (which includes partial and complete unloading). Temperature (in the core of the specimen) and strain evolutions were recorded. Moreover, Young modulus, autogenous and thermal strains have also been measured. Semi-adiabatic tests were also performed which allows for identifying the normalized chemical affinity and associated release of heat (see Eq. 1 and 2).

Basic creep parameters have been identified on experimental evolutions. For the OC, two identifications have been realized. In the first identification, temperature effect on creep is not

taken into account. Corresponding basic creep parameters (see § 2.3) are given in Table 3. In the second identification, temperature effect on basic creep is taken into account. Corresponding basic and transient thermal creep parameters (see § 2.3) are given in Table 4. It should be noticed that the parameter which governs transient thermal creep (λ , see Eq. 22) is less important for the HPC than the OC. Indeed, it is well know that drying and thermal transient creep strains are less important for such a kind of materials. Moreover, if transient thermal creep parameters ($\lambda = 1.38\times10^{-12}$, see Tab. 4) have been considered to be equal for both materials, predicted strains would have overcame experimental data for the HPC.

The comparison between experimental and numerical simulations is given in Figure 11 for the OC, without taking into account effect of temperature on creep (material parameters given in Table 3). Figures 12 and 13 display experimental and simulated evolutions of strain for the OC and HPC, when temperature effect on creep is taken into account (material parameters given in Table 4). For the OC, Laplante (1993) measured a maximal temperature inside the specimen (due to heat release) of about 32°C, as the exterior and initial temperatures were both equal to 20°C. Therefore, the effect of temperature on creep strain evolution is not important, as it can be seen in Figure 12. The adopted model gives good agreement when the specimen is loaded.

As expected, these results underline the fact that creep strains are significant at early-age and should be taken into account. Similar results have been obtained with these experimental results with others uniaxial creep models (Guénot-Delahaie et *al.* 1996). Besides, it seems reasonable to assume that the retardation times are constant at early-age.

In order to compare basic creep of both concretes, delayed strains are plotted in Figure 14 (using identified material parameters of Table 4) for a constant loading (1 MPa) and a

constant temperature (20°C) at different ages of loading (1, 3, 7, 14 and 28 days). As expected, the OC specimen creeps more than the HPC one. Therefore, relaxation of induced stresses will be also less important for the HPC.

3.4 Mechanical simulations of the wall

We assume a perfect binding between the concrete wall and the concrete slab. The slab model is assumed to be visco-elastic (without further hydration). The strain field is assumed to be planar, since the wall is long, with respect to others dimensions. The other mechanical parameters are given in Table 5. Only a 2D calculation is performed. Faria et *al.* (2006) found that 2D and 3D calculations give very close results for their analysis of a massive slab. In order to show the importance of creep strains at early-age, numerical simulations are performed with and without taking into account basic creep strains. Moreover, the effect of temperature on creep strains is also studied.

Since the strains are assumed to be planar, strains perpendicular to the plan ε_{zz} (Figure 5) are fully restrained. Therefore, due to autogenous shrinkage and cooling, tensile stresses are expected to rise. The evolutions of corresponding stresses σ_{zz} at the centre of the wall (dot #3, see Figure 5 for the location) are plotted in Figure 15 and 16 for the OC and the HPC, respectively. Vertical stresses σ_{yy} (centre: dot #3 & #A, see Fig. 5) are compared to tensile strength in Figure 17 for the OC, in order to quantify the effect of temperature gradient. The damage field after 300 hours is displayed in Figure 18 for both concrete.

From these figures, the following results can be drawn:

- At the beginning, compressive stresses σ_{zz} rise, due to the restrain of thermal dilatation. After the temperature decreases in the core, tensile stresses occur at about 64 hours and

70 hours, for the OC and the HPC, respectively. Therefore, basic creep strain in tension must be known precisely from that moment for such a massive structure. Østergaard et *al.* (2001) report drastic change of creep strain at very early-age (i.e. 0.67 & 1 day) which cannot be predicted in available models. It seems that this not a short-coming, since tensile creep strains tend to relax significantly stresses only after several days;

- Tensile stresses occur sooner (about a few hours) when creep is taken into account. This is a negative effect of creep, but at this time, this has no significant effect in term of cracking;
- When temperature effect on creep is not taken into account, creep strains relax slightly stresses below 100 hours. Relaxation becomes important only after 100 hours. The variation of temperature increases significantly creep strains in the OC wall, since a much more important relaxation of stresses is noticed. Indeed, temperature evolves significantly in the structure. However, at this time, stresses overcome already the tensile strength (after 82 and 94 hours for the OC and the HPC, respectively). Therefore, cracking occurs in the wall. Taking into account of effect of temperature on creep strains does not influence significantly time at cracking, but reduces damage values in the wall;
- The predicted tensile stresses and damage values are more important for the OC. Nevertheless, it should be noticed that, for same structures (size, initial and boundary conditions), cracking occurrence depends essentially on temperature variations, Young modulus and creep strains. Therefore, the difference of behaviour between OC and HPC could not be guessed without such type of calculations;

- The computations predict cracking for both concrete, even if creep is taken into account. However, on the site, 7 major crossing cracks have been recorded for the OC, as only one for the HPC (Figure 19, Ithurralde, 1989). It suggests performing rather a 3D calculus in order to evaluate more accurately the occurrence of cracking (at least the number of cracks) and collecting reliable experimental data on creep (which are available, yet);
- The temperature decreasing was, in reality, faster for the OC (see Fig. 7). Therefore, predicted stresses are surely underestimated, since creep strains will be less important;
- Thermal gradient inside the wall is not sufficient to produce vertical cracks. Indeed, a difference of only about 10°C between dot #3 and #4 has been measured. Lykke et *al*. (2000) showed from measurements on an immersed tunnel, that early-age cracking due to thermal gradient occurs only if a temperature difference (between the core and the surface) exceeds about 15 to 20°C.

3.5 Mechanical simulations of the nuclear containment

Numerical simulations are now performed in order to predict cracking occurrence during the construction of concrete containments of a nuclear power plant. A three meters high and 1.2 meter width cylindrical containment part is calculated. It corresponds to one lift. The numerical simulations correspond to the cast of the containment at an advanced stage. A part of the containment, being hardening, is perfectly bounded with a 12 meters high cylindrical wall previously cast and bound on a slab of three meters width.

The geometry and the boundary conditions are given in Figure 20. The calculations are performed during 15 days (duration between lifts). Axisymmetry conditions are used. Initial and ambient temperatures are taken equal to 20°C. Previously identified parameters are used.

The temperature field, after 40 hours, is given in Figure 21. The damage fields in the structure, after 15 days, are displayed on Figure 22, whether temperature effect on creep is taken into account or not.

During lifts, numerical simulation shows that damage occurs in the core of the containment where temperature variation is the most important (in the case where temperature effect on creep is not included). This is due to the restrain induced by the lower containment, which has been previously cast. When temperature effect on creep is included, minor damage is predicted for both OC and HPC. However, as reported in Figure 23, the orthoradial stresses in the core of the OC containment are very close to the tensile strength (2.5 MPa). Since creep parameters have been identified on a different concrete, one must be very careful concerning the obtained results. However, this underlines again the crucial role playing by creep and effect of temperature on the prediction of cracking for such a massive structure.

4. CONCLUSIONS

A finite element model for the prediction of cracking at early-age in massive structures has been developed. This model takes into account thermal diffusion, hydration and subsequent release of heat, autogenous and thermal shrinkage, (basic and thermal transient) creep and cracking (elastic damage). The implementation of the mechanical part of the model in a finite element code is straightforward, since all equations are defined analytically; therefore, no local iterations are needed, which allows for fast calculations. Besides, due to the use of Kelvin-Voigt elements, it is not necessary to store the stress history for the calculations of creep strains.

Numerical simulations have been performed at the scale of specimens and structures, for 2 concrete mixes. The main results obtained from this study can be summarized as follows:

- The time retardation associated to basic creep can be kept constant, as suggested by de Schutter (1999). Aging Kelvin-Voigt elements are found to describe correctly early age creep of concrete (even if concrete is partially or totally unloaded);

- Basic and thermal transient creep strains relax significantly stresses only after several days in massive structure. At this time, cracking has already occurred. Therefore, creep does not delay time at cracking so much, but rather decrease the amplitude of damage (cracking). Besides, the effect of temperature on creep is underlined;

- Minor damage values are found to rise in concrete containments of nuclear power plant during the construction. However, an experimental study is needed, since creep parameters have been indentified on different concretes. Besides, the use of a more realistic phasing of the construction and the study of particular areas (access airlock, corbels…) have to be performed in order to complete this study;

Actually, the use of a more representative cracking model (which includes orthotropy and inelastic strains) is undertaken. Besides, the use of a stochastic approach is also planned, in order to take into account the intrinsic variability of material parameters.

4. REFERENCES

Aggoun, S., Torrenti, J.-M., Legrand, M. and Prost J., 1994. Study of cracking of concrete in tunnels. Annales de l'institut technique du bâtiment et des travaux publics 526, 4-28. (in french)

Arthanari, S. and Yu, C. W., 1967. Creep of concrete under uniaxial and biaxial stresses at elevated temperatures. Mag. of Concrete Res. 19(60), 149–156.

Atrushi, D.S. 2003. Tensile and compressive creep of young concrete: testing and modeling. Norwegian University of Science and Technology, Faculty of Engineering.

Ayotte, E., Massicotte, B., Houde, J. and Gocevski V., 1997. Modeling the thermal stresses at early ages in a concrete monolith. ACI Materials Journals 94(6), p577-587.

Bažant, Z. P. and Wu, S. T., 1974. Rate-type creep law of ageing concrete based on Maxwell chain. Mater. Struct. 7, 45–60.

Bazant, Z. P. 1988. Mathematical modeling of creep and shrinkage of concrete, Wiley, New York.

Bažant, Z.P. and Prasannan, S., 1989. Solidification theory for concrete creep I. Formulation. Journal of Engineering Mechanics 115 (8), 1691-1703.

Bažant, Z.P., Hauggaard, A.B., Baweja, S. and Ulm, F.J., 1997. Microprestress-solidification theory for concrete creep. I: Aging and drying effect. Journal of Engineering Mechanics. 123 (11), 1188-1194.

Bjøntegaard, Ø., 1999. Thermal Dilation and Autogenous Deformation as Driving Forces to Self-Induced Stresses in High Performance Concrete. Doctoral thesis, NTNU, Dept. of Structural Eng.

Byfors, J., 1980. Plain concrete at early ages. Royal institute of technology, PhD.

Cast3m, Commissariat à l'Energie Atomique CEA - DEN/DM2S/SEMT, Cast3m finite element code, available at http://www-cast3m.cea.fr/

Cervera, M., Oliver, J. and Prato, T., 1999. Thermo-chemo-mechanical model for concrete. I: Hydration and aging. J Eng Mech 125(9), 1018–27.

Cervera, M. and Chiumenti, M., 2006. Mesh objective tensile cracking via a local continuum damage model and a crack tracking technique. Computat. Methods Appl. Mech. Engrg. 196, 304-320.

D'Aloïa, L. and Chanvillard, G., 2002. Determining the ''apparent'' activation energy of concrete Ea—Numerical simulations of the heat of hydration of cement. Cement and Concrete Research 32(8), 1277-1289.

de Borst, R. and van den Boogaard, A., 1995. Finite-element modelling of deformation and cracking in early-age concrete. J Eng Mech 120(12), 2519–34.

De Larrard, F., Acker, P. and Ardisson, A., 1992. Genesis and properties of materials. Simulation of its behavior in the structure. Annales de l'IPTBTP 87-104. (in french)

De Schutter, G. and Taerwe, L., 1996. Degree of hydration based description of mechanical properties of early-age concrete. Materials and Structure 29, 335-344.

De Schutter, G. and Taerwe, L., 1997. Fracture energy of concrete at early ages. Materials and Structures 30, 67-71.

de Schutter, G., 1999. Degree of hydration based Kelvin model for the basic creep of early age concrete. Materials and Structures 32, 260-265.

de Schutter, G., 2002a. Finite element simulation of thermal cracking in massive hardening concrete elements using degree of hydration based material laws. Computers and Structures 80, 2035-2042.

De Schutter; G., 2002b. Fundamental study of early age concrete behaviour as a basis for durable concrete structures. Materials and Structures 35, 15-21.

Faria, R., Azenha, M. and Figueiras, J.A., 2006. Modelling of concrete at early ages: Application to an externally restrained slab. Cement and Concrete Composites 28, 572–585

Guenot, I., Torrenti, J.M. and Laplante, P., 1996. Stresses in early age concrete: comparison of different creep models. ACI Materials Journal 93(3), 254-259.

Gutsch, A.-W., 2002. Properties of early-age concrete – Experiments and modeling. Materials and Structures 35, 76-79.

Hattel, J.H. and Thorborg, J., 2003. A numerical model for predicting the thermo-mechanical conditions during hydration of early-age concrete. Applied Mathematical Modelling 27, 1–26.

Hauggaard, A. B., Damkilde, L. and Hansen, P. F., 1999. Transitional thermal creep of early age concrete. Journal of Engineering Mechanics 125(4), 468-465.

Ithurralde, G., 1989. The permeability observed by the prescriber, Colloque Béton à hautes performances, Ecole Normale Supérieure, Cachan. (in french)

Lackner, R., and Mang, H.A., 2004. Chemoplastic material model for the simulation of early-age cracking: From the constitutive law to numerical analyses of massive concrete structures. Cement and Concrete Composites 26, 551–562.

Laplante, P., 1993. Mechanical properties of hardening concrete: compared analysis of normal and high strength concretes. PhD thesis, ENPC, Paris.

Laplante, P., and Boulay, C., 1994. Evolution of coefficient of thermal expansion of concrete with respect to its maturity at very early ages . Materials and Structures 27, 596-605. (in french)

Lokhorst, S.J., and Breugel, K., 1997. Simulation of the effect of geometrical changes of the microstructure on the deformational behavior of hardening concrete. Cement Concrete Research 27(10), 1465–79.

Loukili, A., Chopin, D., Khelidj, A., and Le Touzo, J.-Y., 2000. A new approach to determine autogenous shrinkage of mortar at an early age considering temperature history. Cement and Concrete Research 30(6), 915-922.

Lykke, S., Skotting, E., and Kjaer, U., 2000. Prediction and control of Early-age cracking: experiences from the Oresund tunnel. Concrete International 22(9), 61-65.

Mabrouk, R., Ishida, T. and Maekawa, K., 2004. A unified solidification model of hardening concrete composite for predicting the young age behavior of concrete. Cement and Concrete Composites 26, 453–461

Mazars, J., 1986. A description of micro and macroscale damage of concrete structures. Engineering Fracture Mechanics 25(5:6), 729-737.

Mazars, J., and Bournazel, J.P., 1996. Modelling of damage processes due to volumic variations for maturing and matured concrete. Concrete: from material to Structure, Arles.

Meschke, G., 1996. Consideration of aging of shotcrete in the context of a 3D viscoplastic material model. Int. J. Num. Meth. Eng. 39, 23–43.

Michaud, P.M., 2006. Toward a chemo-poro-visco-elastic approach for the behavior of concrete at early-age. PhD thesis, INSA de Lyon, Lyon. (in french)

Mounanga, P., Baroghel-Bouny, V., Loukili, A., and Khelidj A., 2006. Autogenous deformations of cement pastes: Part I. Temperature effects at early age and micro–macro correlations. Cement and Concrete Research 36, 110– 122

Niu, Y-Z, Tu, C-L, Liang, R-Y, and Zhang, S-W., 1995. Modelling of thermomechanical damage of early-age concrete. J.of Eng. Mech. 121(4), 717–26.

Ostergaard. L., Lange, D.A., Altoubat, S.A., and Stang, H., 2001. Tensile basic creep of early-age concrete under constant load. Cement and Concrete Research 31, 1895-1899.

Pichler, C., Lackner, R., and Mang, H. A., 2007. A multiscale micromechanics model for the autogenous shrinkage deformation of early-age cement-based materials. Engineering Fracture Mechanics 74, 34–58

Pijaudier-Cabot, G., and Bažant, Z.P., 1987. Nonlocal damage theory. J. of Engrg. Mech. 113, 1512-1533.

Regourd, M., and Gauthier, E., 1980. Behavior of cement submitted to accelerate hardening. Annales de I'ITBTP 179, 65-96. (in French)

Rots, J.G., 1988. Computational modeling of concrete fracture. PhD Dissertation, Netherlands; Delft University of Technology.

Sarkis, M., Granju, J.-L., Arnaud, M., and Escadeillas, G., 2002. Coefficient of thermal expansion of a fresh mortar. Materials and Structures 35(251), 415-420.

Schindler, A. K., 2004. Effect of temperature on hydration of cementitious materials. ACI Mat. J. 101(1), 72-81.

Springenschmidt, R., 1998. Prevention of Thermal Cracking in Concrete at Early Ages –State of the Art Report, London, E&FN Spon.

Thelandersson, S., 1987. Modelling of combined thermal and mechanical action in concrete. Journal of Engineering Mechanics 113, 893-903.

Torrenti, J.-M., and Benboudjema, F., 2005. Mechanical threshold of concrete at an early age. Materials and Structures 38(277), 299-304.

Turcry, P., Loukili, A., Barcelo, L., and Casabonne, J. M., 2002. Can the maturity concept be used to separate the autogenous shrinkage thermal deformation of cement paste at early age? Cement and Concrete Research, 32(9), 1443-1450.

Ulm, F.-J., and Coussy, O., 1998. Couplings in early-age concrete: from material modelling to structural design. International Journal of Solids and Structures 35(31-32), 4295-4311.

Waller, V., 2000. Relationship between concrete mix, exothermy during the setting and compressive strength. Collection Etudes et recherches des Laboratoires des Ponts et Chaussées, série « Ouvrages d'Art », OA35 – LCPC, Paris. (in French)

Waller, V., d'Aloïa, L., Cussigh, F., and Lecrux, S., 2004. Using the maturity method in concrete cracking control at early ages. Cement and Concrete Composites 26, 589–599.

Xiang, Y., Zhang, Z., He, S., and Dong G., 2005. Thermal–mechanical analysis of a newly cast concrete wall of a subway structure. Tunnelling and Underground Space Technology 20, 442–451.

4. NOMENCLATURES

ξ hydration degree;

$\tilde{A}(\xi)$ normalized affinity;

E_a activation energy [J.mol^{-1}];

R constant of perfect gas [8.314 J.mol^{-1}.K^{-1}];

T temperature [K];

L latent heat of hydration [J.m^{-3}];

k thermal conductivity [$W.m^{-1}.K^{-1}$];

C volumetric heat capacity [$J.m^{-3}.K^{-1}$];

$\boldsymbol{\varphi}$ heat flux [$W.m^{-2}$];

h coefficient of exchange by convection [$W.m^{-2}.K^{-1}$];

T_s temperature on the surface [K];

T_{ext} ambient temperature [K];

$\boldsymbol{\varepsilon}_{au}$ autogenous shrinkage;

$\mathbf{I}$ second order unit tensor;

$\mathbf{1}$ unit vector;

κ constant material parameter governing autogenous shrinkage;

$\boldsymbol{\sigma}$ apparent stresses [Pa];

$\tilde{\boldsymbol{\sigma}}$ effective stresses [Pa];

D damage;

$\mathbf{E}$ elastic stiffness tensor [Pa];

$\boldsymbol{\varepsilon}_e$ elastic strains;

$\boldsymbol{\varepsilon}_{bc}$ basic creep strains;

$\boldsymbol{\varepsilon}_{ttc}$ transient thermal creep strains;

$\boldsymbol{\varepsilon}$ total strains;

ξ_0 mechanical percolation threshold [0.1];

ξ_∞ final hydration degree;

E_∞ final Young modulus [Pa];

β constant governing the evolution of Young modulus with respect to hydration degree [0.62];

$\hat{\varepsilon}$ elastic equivalent tensile strain;

f damage criterion;

$\kappa_0(\xi)$ tensile strain threshold;

A_t, B_t constant material parameters controlling softening in tension;

$f_t(\xi)$ tensile strength [Pa];

$f_{t\infty}$ final tensile strength [Pa];

γ constant governing the evolution of tensile strength with respect to hydration degree [0.46];

g_{ft} dissipated energy density at failure in tension [J.m^{-3}];

G_{ft} fracture energy [J.m^{-2}];

l_c characteristic length [m];

δ constant governing the evolution of fracture energy with respect to hydration degree [0.46];

$\tilde{\sigma}_{ds}^{i}$ effective stresses acting on the dashpot in the Kelvin-Voigt unit *i*;

$\tilde{\sigma}_{sp}^{i}$ effective stresses acting on the spring in the Kelvin-Voigt unit *i*;

k_{bc}^{i} stiffness of the spring in the Kelvin-Voigt unit *i*;

η_{bc}^{i} viscosity of the dashpot in the Kelvin-Voigt unit *i*;

$k_{bc\_\infty}^{i}$ final stiffness of the spring in the Kelvin-Voigt unit *i*;

τ_{bc}^{i} retardation time associated to the Kelvin-Voigt unit *i*;

E_{ac} creep activation energy [17.4 kJ.mol^{-1}];

T_0 reference temperature [293 K];

λ material parameter governing transient thermal creep [Pa^{-1}.K^{-1}];

t time [s];

a_{bc}, b_{bc}, c_{bc} basic creep parameters;

$\mathbf{A}_{bc}$, $\mathbf{B}_{bc}$, $\mathbf{C}_{bc}$ second order basic creep tensors;

t_{ttc} thermal transient creep parameter;

$\mathbf{T}_{ttc}$ second order thermal transient creep tensor;

$\mathbf{E}_c$ elastic stiffness tensor corrected by creep [Pa];

Subscripts

0 initial value;

~ effective quantity;

n value at time t_n;

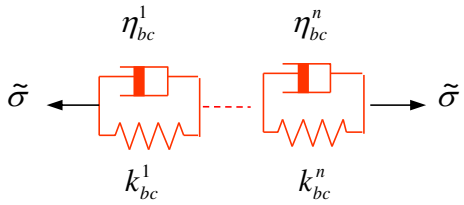

Figure 1. Kelvin-Voigt elements for the prediction of creep strains.

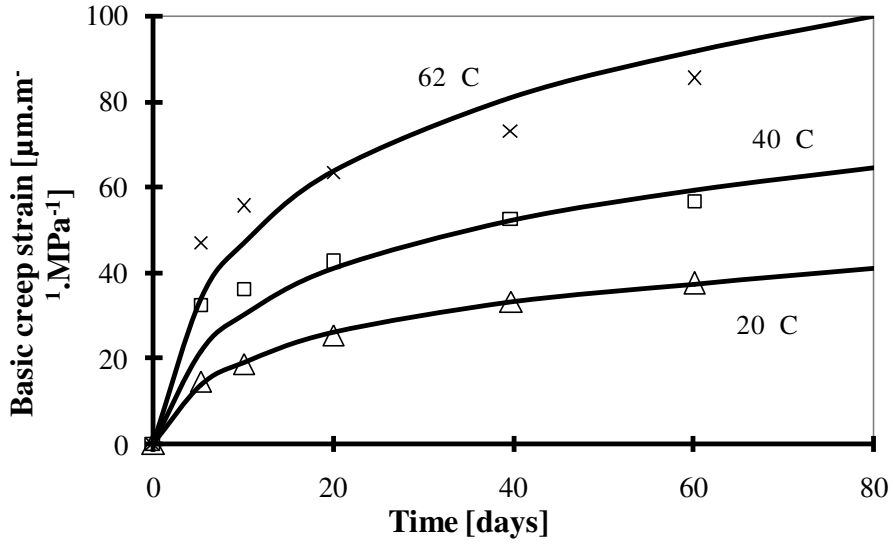

Figure 2. Basic creep strain evolution for different constant temperatures (experimental results are from Arthanari and Yu, 1967).

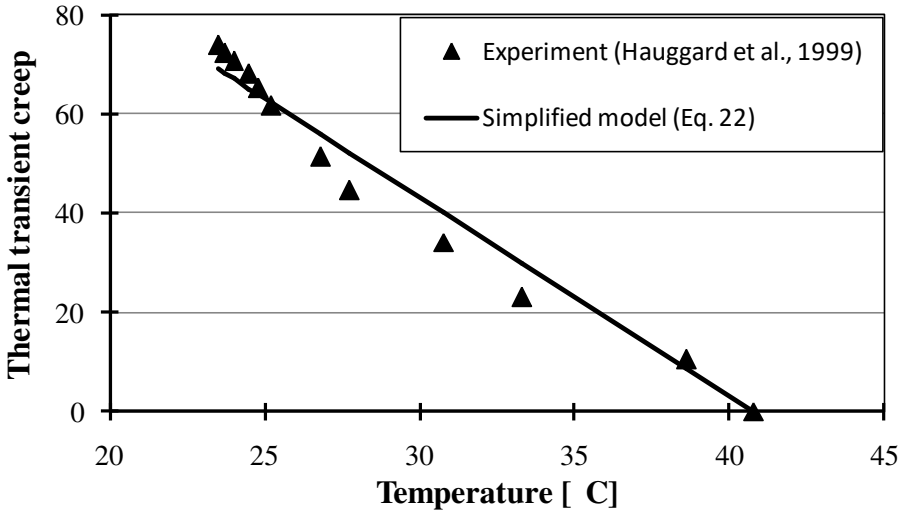

Figure 3. Evolution of thermal transient creep strains: comparison between experimental data (Hauggard et *al.*, 1999) and used simplified model (Eq. 22). The specimen was loaded 16 h after mixing with 2.9 MPa corresponding to 29% of the compressive strength.

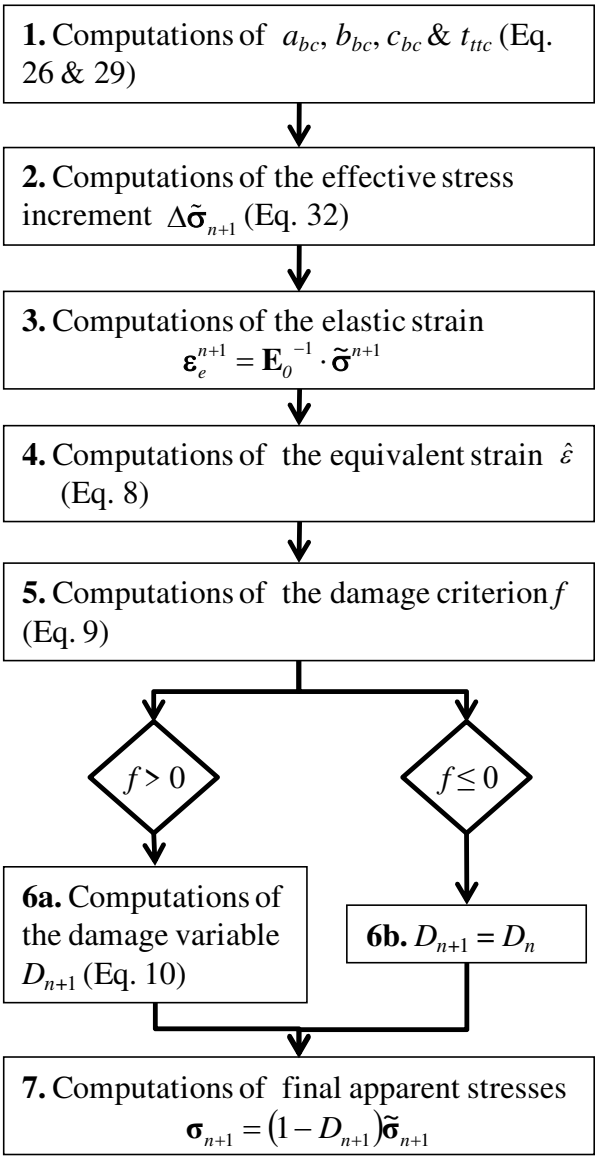

Figure 4. Local algorithm.

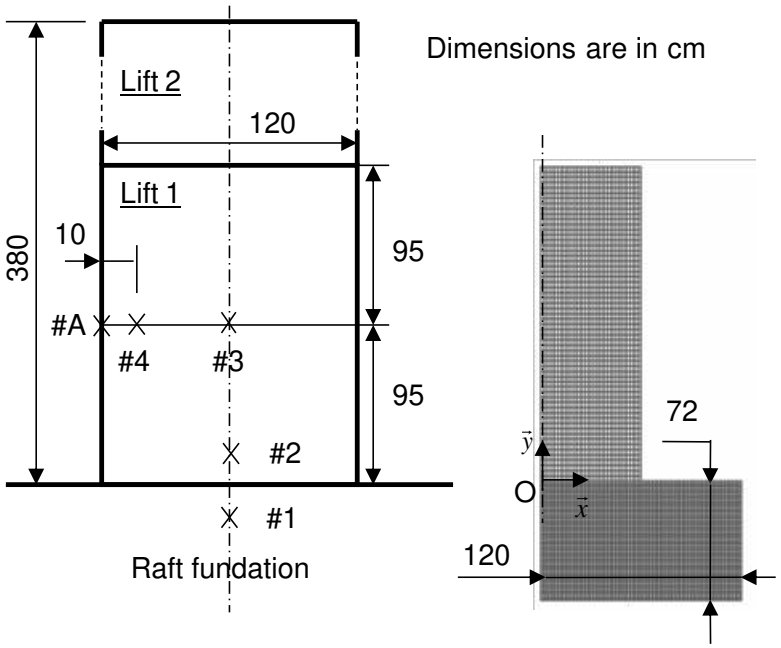

Figure 5: Geometry and finite element mesh of the wall – locations of the thermocouples (#1, #2, #3 & #4). Due to symmetry, only half of the wall is meshed.

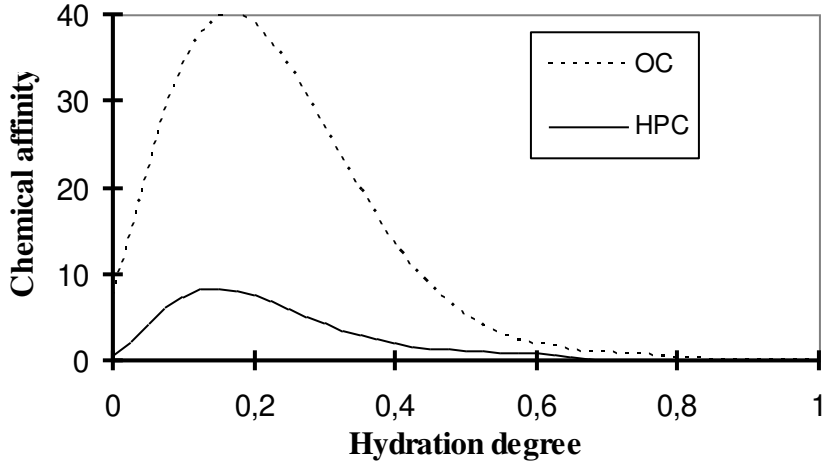

Figure 6: Evolution of normalized chemical affinity (Eq. 1) with respect to hydration degree.

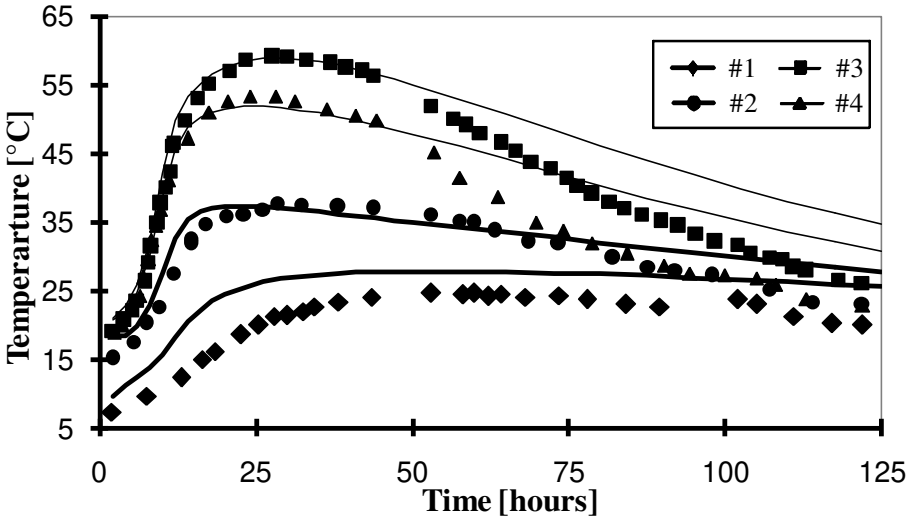

Figure 7: Comparison between experimental and simulated evolutions of temperature in the wall for the OC at different locations (see Fig. 5).

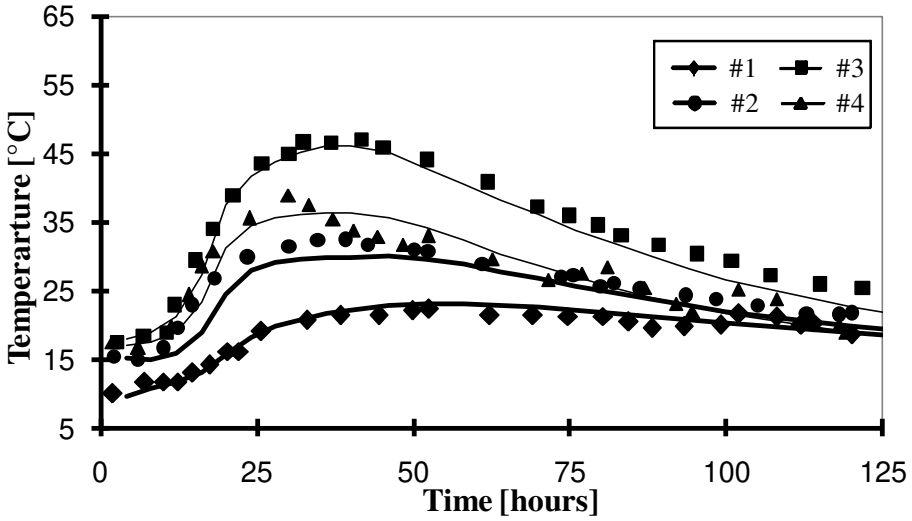

Figure 8: Comparison between experimental and simulated evolutions of temperature in the wall for the HPC at different locations (see Fig. 5).

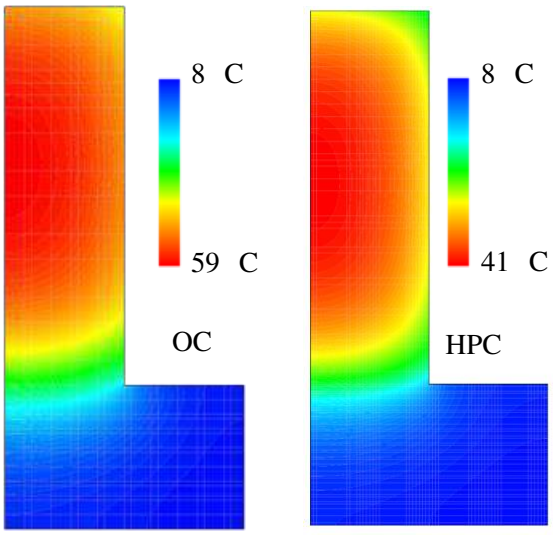

Figure 9: Temperature field inside OC and HPC walls after 25 hours.

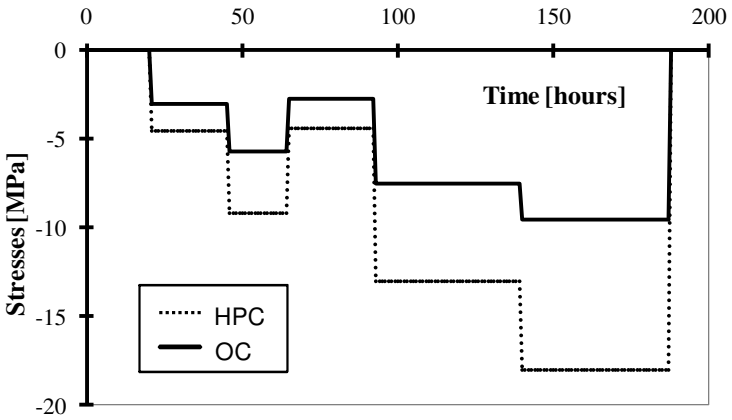

Figure 10: Stress history applied on OC and HPC concretes (Laplante and Boulay, 1994).

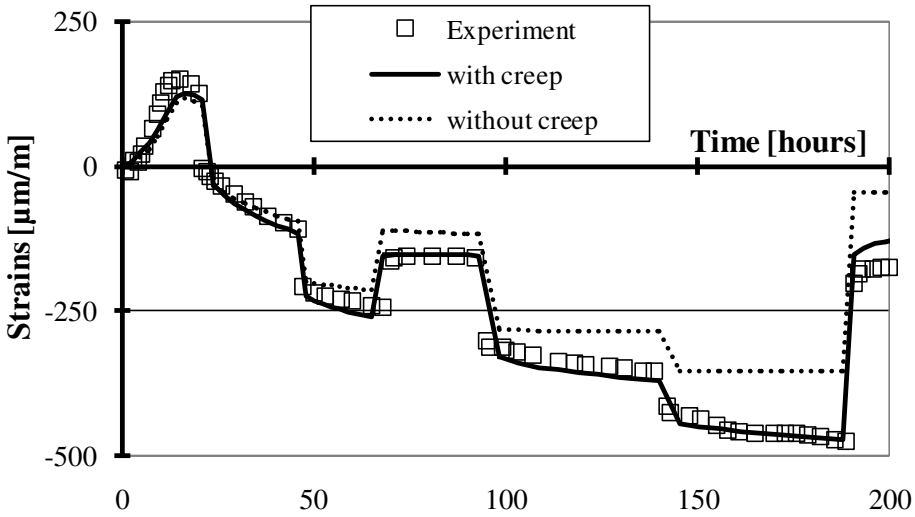

Figure 11: Comparison between experimental and simulated evolutions of strains (without and with creep) for the OC (with material parameters given in Table 3). Effect of temperature is not taken into account.

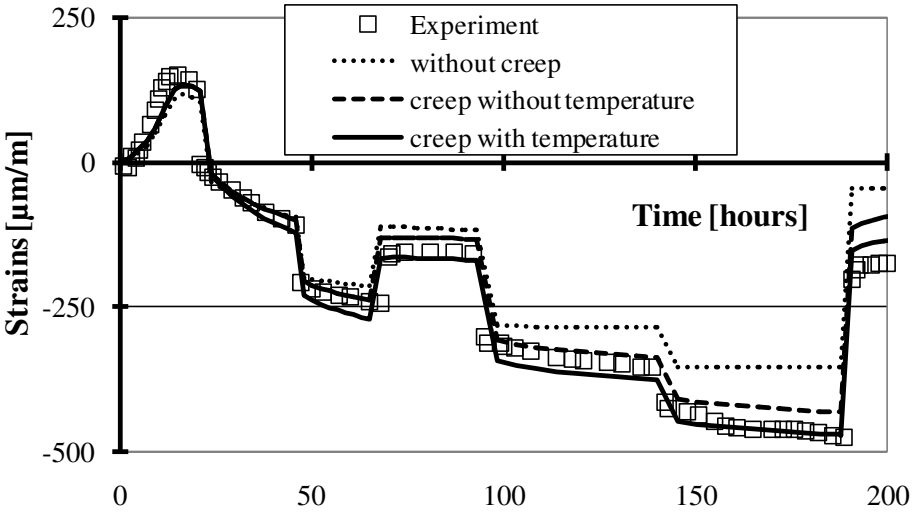

Figure 12: Comparison between experimental and simulated evolutions of strains (without and with temperature effect on creep) for the OC (with material parameters given in Table 4).

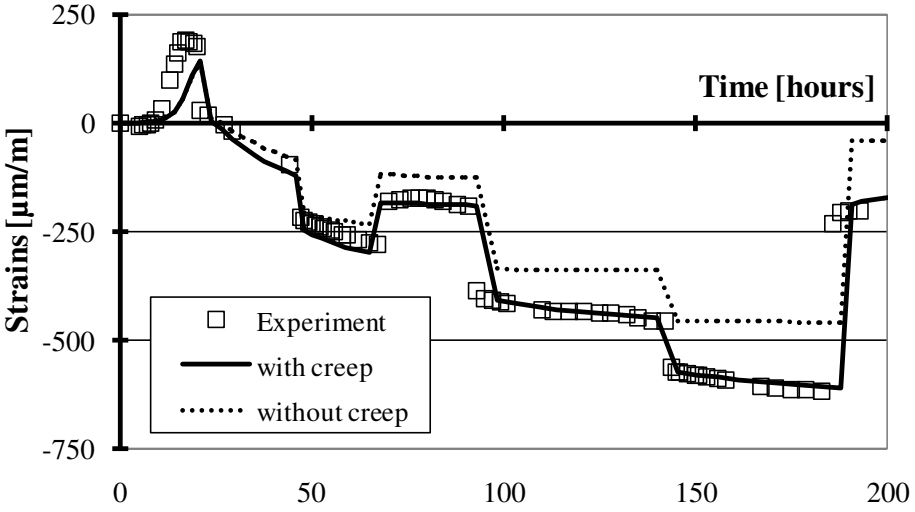

Figure 13: Comparison between experimental and simulated evolutions of strains (without and with creep) for the HPC (with material parameters given in Table 4). Effect of temperature is taken into account.

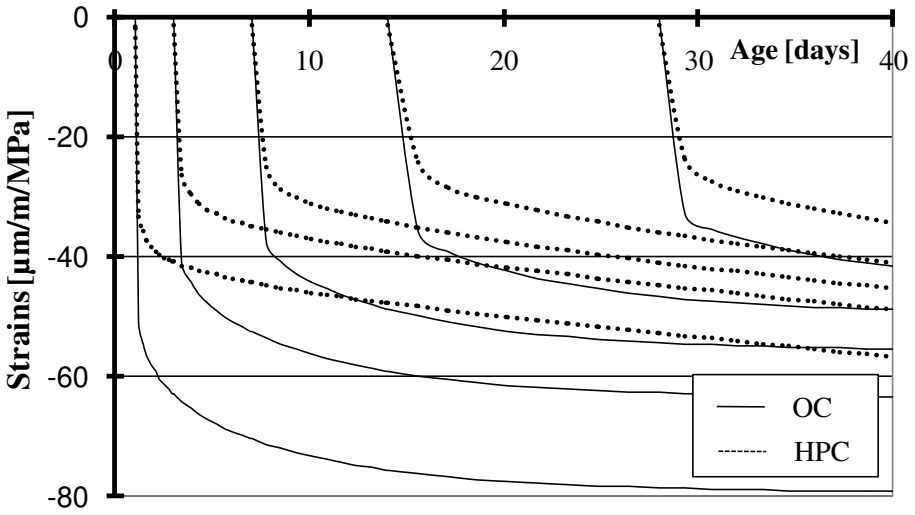

Figure 14: Delayed strains for a constant loading (1 MPa) and an constant temperature (20°C) at different loading ages (1, 3, 7, 14 and 28 days) of the OC and the HPC.

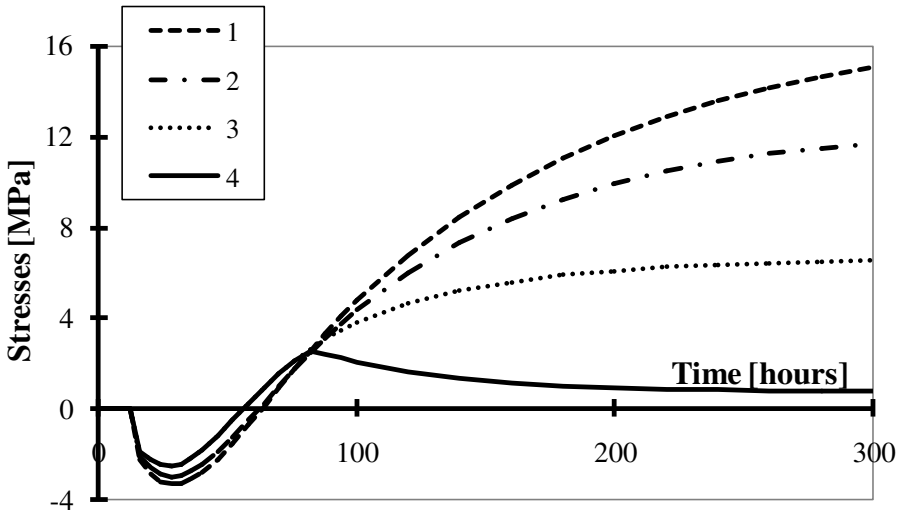

Figure 15: Evolution of stresses σ_{zz} at the centre of the structure (dot #3, see Fig. 5) with respect to time for the OC. (1 = Elastic model, 2 = elastic model + creep without taking into account effect of temperature, 3 = elastic model + creep with account of temperature effect, 4 = damage model + creep with account of temperature effect)

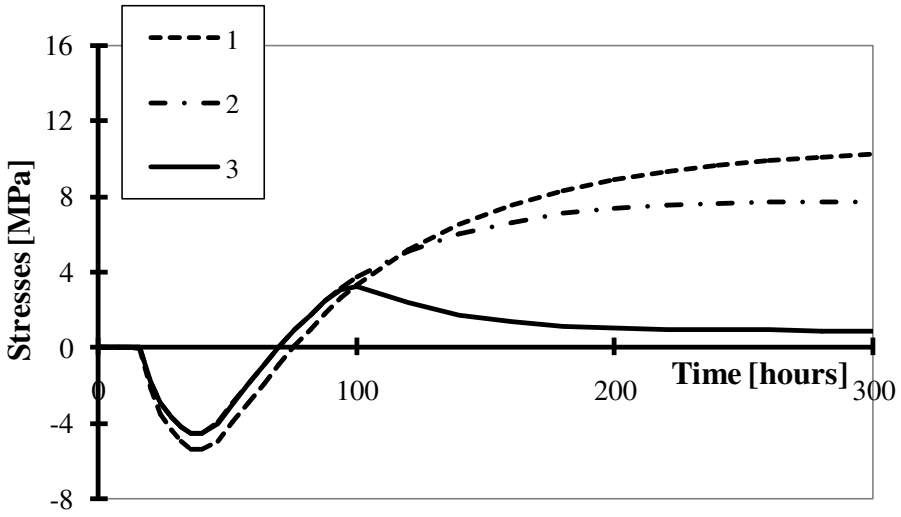

Figure 16: Evolution of stresses σ_{zz} at the centre of the structure (dot #3, see Fig. 5) with respect to time for the HPC. (1 = Elastic model, 2 = elastic model + creep with account of temperature effect, 3 = damage model + creep with account of temperature effect)

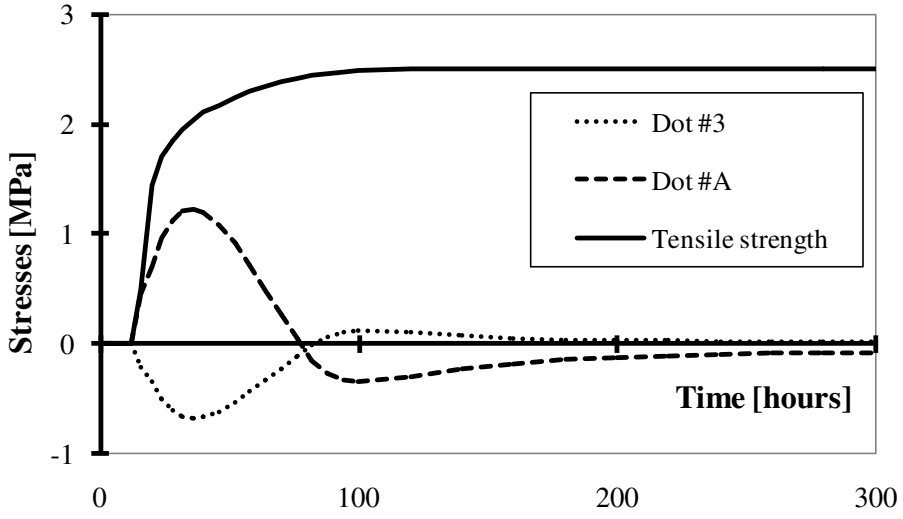

Figure 17: Evolution of stresses σ_{yy} at the centre and the surface of the structure (dot #3 & #A, see Fig. 5) with respect to time for the OC.

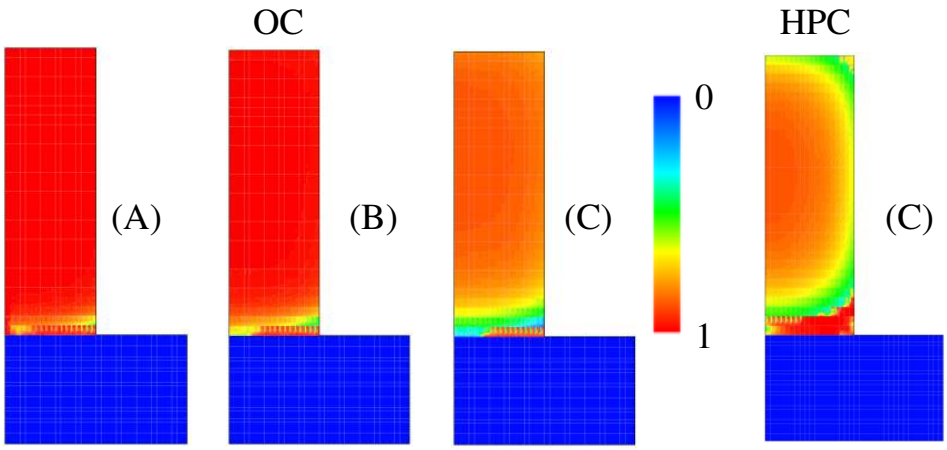

Figure 18: Damage field in the wall after 300 hours: A = Damage model only, B = Damage model with creep without taking into account effect of temperature, C = Damage model with creep with account of temperature effect.

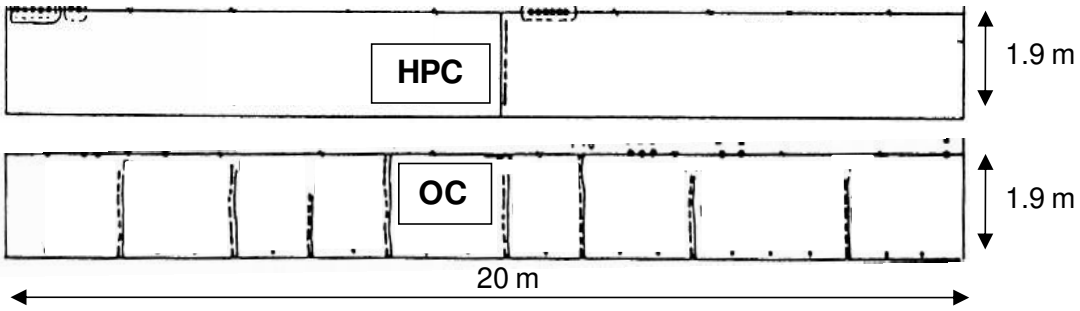

Figure 19: Cracking pattern of OC (at the bottom) and HPC (at the top) walls in site (Ithurralde, 1989). The cracks are represented by a straight line. 8 major cracks have been noticed of the OC (1×40 µm + 4×100 µm + 2×200 µm + 1×500 µm). 1 major cracks has been noticed for the HPC (1×100 µm).

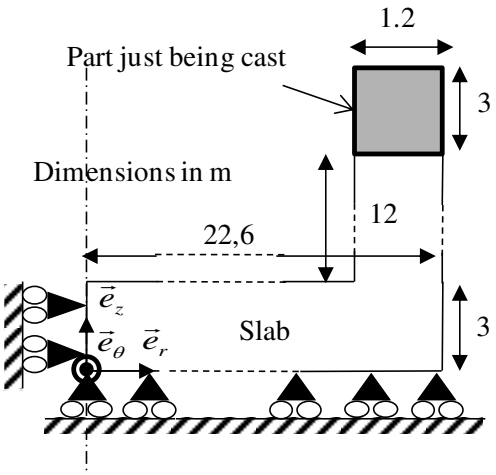

Figure 20: Geometry and boundary conditions of the containment.

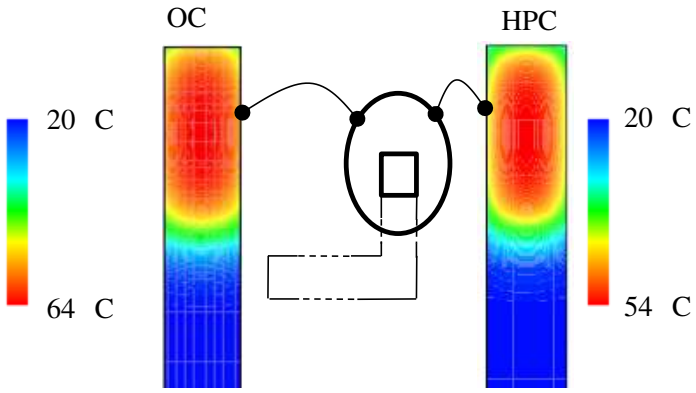

Figure 21: Temperature field in the containments after 40 hours.

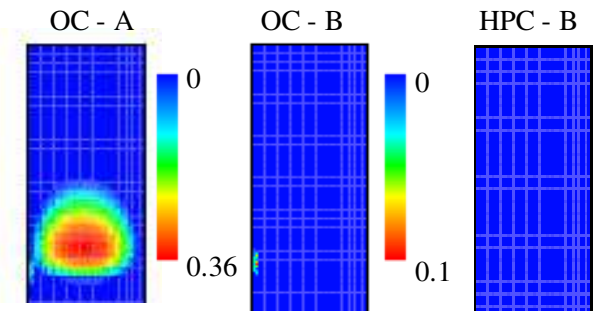

Figure 22: Damage field at the top of the containment (see Fig. 20) after 15 days (A = Damage model with creep without taking into account effect of temperature, B = Damage model with creep with the take into account of temperature effect).

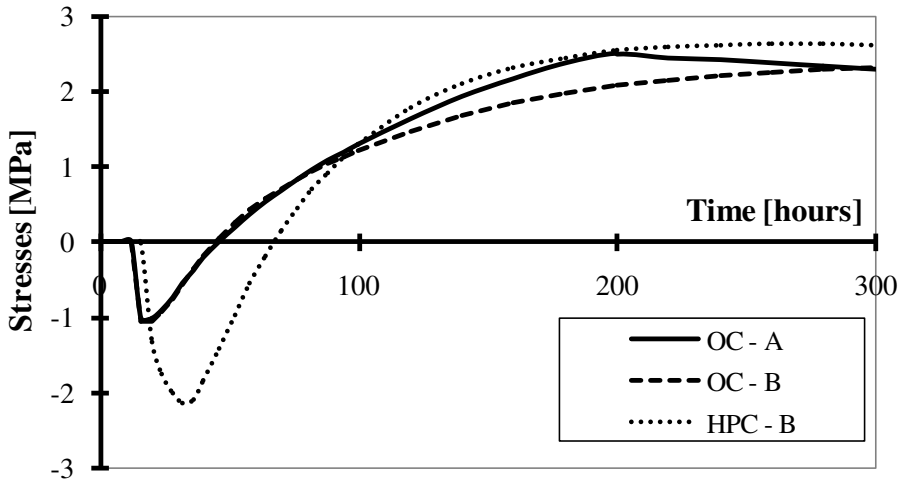

Figure 22: Evolution of orthoradial stresses $\sigma_{\theta\theta}$ in the centre of the structure with respect to time for the OC and HPC (A = Damage model with creep without taking into account effect of temperature, B = Damage model with creep with the take into account of temperature effect).

Table 1: mix of concretes (Ithurralde, 1989).

	Aggregates [kg.m^{-3}]		Sand [kg.m^{-3}]	Cement CEM II/A 52.5 (CPJ 55 PM) [kg.m^{-3}]	Limestone Filler [kg.m^{-3}]	Silica fume [kg.m^{-3}]	water-reducing plasticizer [L.m^{-3}]	Water [L.m^{-3}]
	12.5/25	5/12.5						
OC	783	316	772	350	-	-	1.04	195
HPC	791	309	759	266	114	40.2	7.68	161

Table 2: thermal parameters.

	h [W.m^{-2}.°C^{-1}]	k [W.m^{-1}.°C^{-1}]	C [J.m^{-3}.°C^{-1}]	L [J.m^{-3}]	E_a/R [°K^{-1}]
OC	3	3.05	2.4×10^6	154.7×10^6	4400
HPC				141.5×10^6	4000

Table 3: Basic creep parameters for OC: effect of temperature on creep has not been taken into account.

	k_{bc}^1 [GPa]	τ_{bc}^1 [days]	k_{bc}^1 [GPa]	τ_{bc}^1 [days]	k_{bc}^1 [GPa]	τ_{bc}^1 [days]
OC	1.3×10^3	0,1	650	1	130	10

Table 4: Creep parameters for OC and HPC: effect of temperature on creep is included.

	k_{bc}^1 [GPa]	τ_{bc}^1 [days]	k_{bc}^1 [GPa]	τ_{bc}^1 [days]	k_{bc}^1 [GPa]	τ_{bc}^1 [days]	λ [$Pa^{-1}.°C^{-1}$]
OC	10^3	0,1	500	1	100	10	1.38×10^{-12}
HPC	3.10^3		1.6×10^3		110		2.76×10^{-13}

Table 4: Mechanical parameters

	κ	α	E_∞ [GPa]	$f_{t\infty}$ [MPa]	A_t	B_t
OC	7.10^{-5}	1.2×10^{-5}	32	2.5	1	17.10^3
HPC	3.10^{-5}		36	3.2		